

Sensitivity Constraints of Extractive Electrospray for a Model System and Secondary Organic Aerosol

David M. Bell,* Jun Zhang, Jens Top, Sophie Bogler, Mihnea Surdu, Jay G. Slowik, Andre S. H. Prevot, and Imad El Haddad



Cite This: *Anal. Chem.* 2023, 95, 13788–13795



Read Online

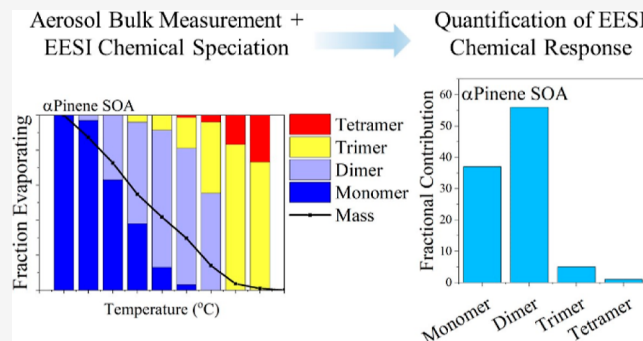
ACCESS |

Metrics & More

Article Recommendations

Supporting Information

ABSTRACT: The quantification of an aerosol chemical composition is complicated by the uncertainty in the sensitivity of each species detected. Soft-ionization response factors can vary widely from molecule to molecule. Here, we have employed a method to separate molecules by their volatility through systematic evaporation with a thermal denuder (TD). The fraction remaining after evaporation is compared between an extractive electrospray ionization time-of-flight mass spectrometer (EESI-TOF) and a scanning mobility particle sizer (SMPS), which provides a comparison between a quantified mass loss by the SMPS and the signal loss in the EESI-TOF. The sensitivity of the EESI-TOF is determined for both a simplified complex mixture (PEG-300) and also for a complex mixture of α -pinene secondary organic aerosol (SOA). For PEG-300, separation is possible on a molecule-by-molecule level with the TD and provides insights into the molecule-dependent sensitivity of the EESI-TOF, showing a higher sensitivity toward the most volatile molecule. For α -pinene SOA, sensitivity determination for specific classes is possible because of the number of molecular formula observed by the EESI-TOF. These classes are separated by their volatility and are broken down into monomers ($O_{3-5,6-7,8+}$), dimers ($O_{4-7,8+}$), and higher order oligomers (e.g., trimers and tetramers). Here, we show that the EESI-TOF initially measures 60.1% monomers, 32.7% dimers, and 7.2% trimers and tetramers in α -pinene SOA, but after sensitivity correction, the distribution of SOA is 37.4% monomers, 56.1% dimers, and 6.4% trimers and tetramers. These results provide a path forward for the quantification of aerosol components with the EESI-TOF in other applications and potentially for atmospheric measurements.



Aerosols are particles suspended in air with diameters spanning from the nanometer to micrometer range.¹ Aerosols are used for drug delivery,² but can be detrimental to human health when they include toxic components (e.g., PAHs, non-exhaust traffic emissions, dust, etc.).³ For both cases, it is important to measure and quantify the chemical components present in the aerosol.⁴ Quantification is particularly difficult for atmospheric organic aerosol (OA), which makes up 20–90% of atmospheric aerosol.⁵ A mixture of directly emitted molecules and species formed from gas-phase oxidation reactions make up the composition of OA. Reactions of emitted molecules with atmospheric oxidants can yield thousands of different product molecules,^{6,7} making quantification with standards an impossible task. Oxidation products can vary significantly in their composition, ranging from low-molecular-weight monomers to high-molecular-weight oligomers (e.g., dimers, trimers, tetramers, etc.). Oligomeric content has been shown to be an important contribution of OA generated in laboratory studies,⁸ but quantification of these products are lacking. Therefore, the importance of oligomers in both laboratory studies and the atmosphere remains uncertain.

Harsh electron impact ionization provides quantitative analysis, but in the complex matrix of OA, electron impact techniques cannot provide molecular information. Soft ionization techniques that include chemical ionization methods (e.g., I^- , NO_3^- , NH_4^+ , H_3O^+ , etc.),^{6,9,10} droplet assisted ionization, and extractive electrospray ionization^{4,11–14} afford detailed chemical resolution, but sensitivity can vary dramatically from molecule to molecule.^{4,11,15} The EESI technique is a soft ionization method with sensitivity toward organic molecules sufficient for atmospheric measurements ($ng\ m^{-3}$ detection limits).^{13,14,16,17} In these studies, the electrospray working solution (water or water/acetonitrile mix) was doped with NaI to promote Na^+ adduct formation and detects molecules that are soluble and have strong binding energies to

Received: January 30, 2023

Accepted: August 11, 2023

Published: September 1, 2023



Na^+ . Though, some fragmentation appears to occur when both hydroxynitrates or nitrate functional groups are present,^{17,18} and other potential artifacts (e.g., reactions) are observed in ESI experiments,¹⁹ but have not been detected within EESI measurements of OA to date.

In pursuit of quantitative analysis from soft ionization techniques, recent studies have constrained the instrument response to a given analyte according to its binding energy to adducts in chemical ionization techniques, which is in turn estimated from the analyte's molecular formula. Gas-particle partitioning has also been attempted as a way to constrain the response factor for the extractive electrospray ionization when compared against a proton-transfer reaction mass spectrometer (PTR-MS) measuring gas-phase species.⁴ This study used a seed aerosol to encourage partitioning of gaseous molecules to the particle phase, but was only sensitive to species the PTR-MS could measure and those that would partition to the aerosol phase. Thus, the predominant species measured were smaller molecules predominantly found in the gas-phase, with no molecules larger than 300 m/z reported. Thus, a significant gap exists in determining the response to oligomeric species and their quantification remains uncertain.

In this study, we provide a new approach to quantify the measured EESI-TOF composition. Here, the EESI-TOF response is compared against bulk organic mass concentration measured by a scanning mobility particle sizer (SMPS) for mixtures of quasi-known species (PEG-300) and a complex mixture of α -pinene SOA. PEG-300 is a group of molecules that spans a wide range in both mass and volatility, and is a common set of molecules used for instrument calibrations.²⁰ The EESI-TOF sensitivity toward classes of compounds with different volatilities is assessed by systematically removing molecules from the aerosol phase via evaporation using a thermal denuder (TD). The technique developed here will be beneficial for the quantification of molecular groups in different complex aerosol mixtures, potentially including in ambient environments or industrial applications, and can be applied to aerosol mass spectrometers other than the EESI-ToF.

■ EXPERIMENTAL SECTION

Laboratory experiments were conducted with both the individual model compounds PEG 5, 6, 8, 10, and 12 and the mixture of PEG-300, and an experimental setup can be found in Figure S1. The solutions were aerosolized using a home-built nebulizer, creating aerosols that were subsequently dried. PEG-300 was introduced to a TD (Aerodyne), with 1.3 L min⁻¹ sampled into the TD and the excess flow exhausted. After the TD, a multi-channel charcoal denuder was installed to remove the gas-phase species that evaporate during heating. Finally, the particles were sampled by the EESI-TOF and a scanning mobility particle sizer (SMPS, TSI Inc. model 3938, 3 L min⁻¹ sheath and 0.3 L min⁻¹ sample). The condensation particle counter (CPC) used was compared against an ACTRIS standard CPC and agreed within $\pm 2\%$. The SMPS was calibrated with a series of polystyrene latex spheres, and agreed well with the manufacturers specifications. The aerosol mass was determined using the assumed particle density of PEG-300 (1.13 g cm⁻³) or α -pinene SOA (1.2 g cm⁻³).^{21,22} Similar particles have been measured previously and were shown to be spherical, removing possible uncertainties in the aerosol mass measurement.²² The multiple charge correction inversion creates the largest uncertainty in the SMPS measurement and is on the order of $\sim 10\%$; therefore, the

absolute error on the mass measurement of the SMPS will be on the order of $\sim 15\%$. The temperature of the TD was systematically increased from low to high temperatures during the course of the experiment. Experiments with nebulizers had relatively constant aerosol concentrations ($\pm 5\%$). The residence time in the TD varied from 7 s at 20 °C to 3.5 s at 175 °C.

Secondary organic aerosol experiments were performed in a 9 m³ atmospheric simulation chamber, described previously.²³ In the experiments presented here, α -pinene SOA was produced by reacting 100 ppb of α -pinene with ~ 1000 ppb of O₃. High concentrations of O₃ were utilized to reach maximum aerosol concentrations within the first 3–5 min after α -pinene injection. In chamber experiments, the particles were sampled either directly from the chamber to the instruments (SMPS, and EESI-TOF) or passed through a longer line including the TD with a multi-channel denuder on the output. The time series were corrected for both chamber dilution and wall loss of particles in the chamber using the same method reported previously.^{10,13}

A subset of measurements was performed with an Orbitrap mass spectrometer (Thermo Fisher, Exploris 120). A PEG-300 solution was nebulized, dried using a Nafion dryer and subsequently introduced into an Orbitrap, equipped with a custom build EESI inlet. MS/MS was carried out for each PEG from 5 to 12, with the collision energy ranging from 1 to 40 eV. Signal at 1 eV was used to normalize the results.

■ EXTRACTIVE ELECTROSPRAY IONIZATION MASS SPECTROMETRY

The EESI was connected to an atmospheric pressure time-of-flight mass spectrometer (Tofwerk) with a resolution of either 5000 ΔM/M (PEG experiments) or 10,500 ΔM/M (smog chamber experiments). The aerosol was passed through a series of switching valves oscillating between a sampling line (5 min) and a HEPA filter (1 min) to continually obtain background measurements. After the series of switching valves, a multi-channel denuder stripped the gas-phase components, ensuring the EESI only encountered the aerosols. The electrospray capillary operated at 2.9 kV with a backing pressure of 0.2 bar with a working solution of 100 ppm NaI in purified water (MilliQ). The inlet to the mass spectrometer consisted of a metal inlet capillary that was typically heated to 270 °C, except for a single PEG-300 experiment at 110 °C. Thermocouples were connected to different points on the EESI inlet (see Figure S2) to assess the temperatures encountered by the particles on entering the instrument. The higher inlet capillary temperature resulted in an EESI temperature of 40 °C (at Figure S2: P2) and an inlet tube temperature (Figure S1: P1) of 35–40 °C, while for the lower inlet capillary temperature (110 °C) both P1 and P2 were 22 °C. The data were analyzed using Tofware v3.2.3. In the experiments with standards and PEGs, all peaks were assigned according to their known polymeric molecular formulae. For α -pinene SOA, peaks could be effectively assigned to species below m/z 500; however, the mass spectrometer resolution prevented conclusive assignments above m/z 500. However, there are significant contributions to the aerosol signal present above m/z 500 and these data are used to determine the signal associated with trimers and tetramers, as discussed below in the Results section. The data are obtained as ions s⁻¹, which were converted to ag s⁻¹ by the following

$$\text{EESI (ag s}^{-1}\text{)}_x = \frac{\text{EESI (# s}^{-1}\text{)}_x \cdot \text{MW}_x \times 10^{18}}{6.023 \times 10^{23}} \quad (1)$$

where $\text{EESI (# s}^{-1}\text{)}_x$ is the measured EESI signal of ion x in s^{-1} , MW_x is the molecular weight of x , Avogadro's number converts molecules into mole, and 10^{18} converts grams into attograms (ag).

RESULTS

Separating Sensitivity in an Ideal Complex Mixture.

PEGs span a wide range of molecular weights, shown in Figure 1A. PEGs are detected as $\text{C}_{2n}\text{H}_{4n+2}\text{O}_{n+1}\text{Na}^+$ because of adduct

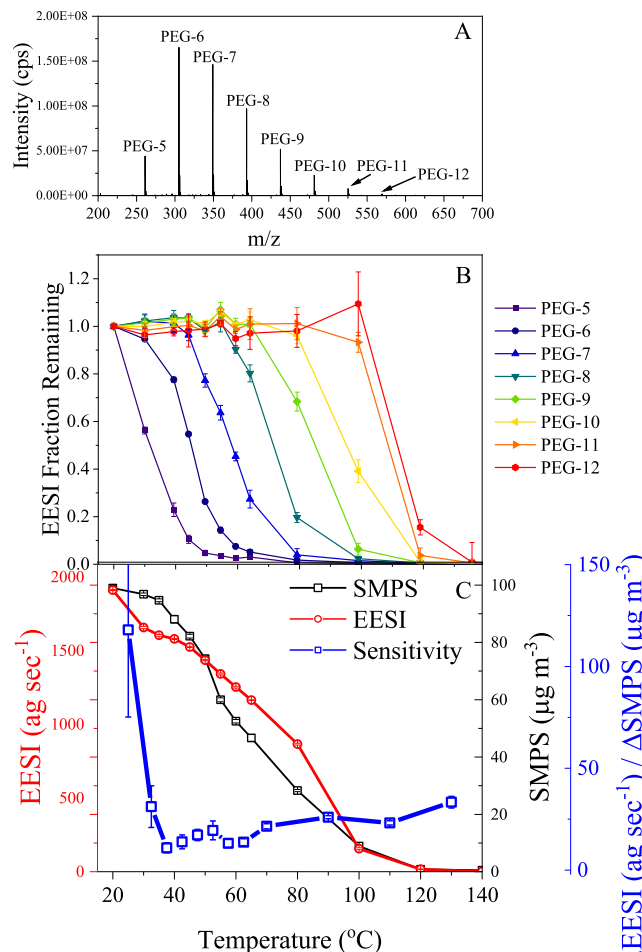


Figure 1. (A) Mass spectrum of PEG-300 as measured by the EESI. (B) Fraction remaining of each PEG measured by the EESI as a function of TD temperature, from triplicates. (C) A single measurement showing absolute mass concentration (left-axis) measured by the SMPS, EESI mass flux (red axis, right side), and for the EESI sensitivity using the mid-point temperatures (blue axis, right side), and the error bars correspond to the error propagated using the measured standard error.

formation with Na^+ in the electrospray solution, and are observed to span $n = 5-16$ by the EESI-TOF ranging from 261 to 745 m/z . A majority (99%) of the signals shown in Figure 1A represent PEG- Na^+ adducts. The range of masses shown in Figure 1A delivers a useful range over which to assess the sensitivity of the EESI-TOF as a function of the molecular weight of species containing the same functional groups.

To isolate the sensitivity on a molecule-by-molecule basis, a TD was used to selectively evaporate molecules based on their saturation vapor concentration (or volatility). The method requires the EESI-TOF to be used in conjunction with a quantitative reference instrument (here, the SMPS is used) because the SMPS provides a quantitative measure of the mass concentration ($\mu\text{g m}^{-3}$) of organics present, while the EESI measures the different molecular formula of species remaining after evaporating the most volatile fraction from the aerosol. Figure 1B shows the relative fraction remaining as a function of TD temperature as measured by the EESI-TOF, and highlights the ability to separate specific molecules from the complex mixture of PEG-300 as a function of TD temperature.

Figure 1C shows the change in the total EESI signal and the measured mass by the SMPS, as a function of temperature (size distributions are shown in Figure S3). There are distinct differences in the temperature dependence exhibited by all measurements, with the EESI undergoing an initial large drop in intensity between 20 and 30 °C, followed by evaporation that appears delayed relative to the SMPS, and matching the SMPS again above 100 °C.

Figure 1C also shows the bulk sensitivity for the $\text{EESI (ag s}^{-1}\text{)} / (\mu\text{g m}^{-3})$, determined by comparing the change in total EESI signal (ag s^{-1}) to the change in mass measured by the SMPS, as follows

$$\text{sensitivity}_{\text{bulk}} = \frac{\sum \text{EESI} (T_1)_i - \sum \text{EESI} (T_2)_i}{\text{SMPS mass} (T_1) - \text{SMPS mass} (T_2)} \quad (2)$$

where T_1 and T_2 are the adjacent TD temperature setpoints, the SMPS mass is the average mass concentration over the measurement period, and $\text{EESI} (T_x)$ is the summed EESI signal for all measured components at a specific temperature. Here, we define the sensitivity in terms of the fraction that is evaporating from the aerosol phase in eq 2.

As shown in Figure 1C, the bulk sensitivity varies considerably as a function of volatility. The sensitivity initially decreases dramatically because there is virtually no change in the signal of the SMPS, while the EESI observes a 15% decrease in signal between 20 and 30 °C. These changes are associated with evaporation of the most volatile PEG ($n = 5$, $\text{C}_{10}\text{H}_{22}\text{O}_5$), which fully evaporates by 40 °C and is detected with unusually high sensitivity. With the increase in temperature, the sensitivity decreases, reaching a minimum between 35 and 50 °C, where PEG-6 ($\text{C}_{12}\text{H}_{26}\text{O}_6$) was the predominant species evaporating. The sensitivity then increased for the larger molecules from 10 to 30 ($\text{ag s}^{-1}\text{)} / (\mu\text{g m}^{-3})$. Figure S4 shows the dominant species evaporating between each temperature step. Where a specific PEG made up 50% of the evaporating fraction, the sensitivity derived from taking an average of the bulk method (shown in Figure 1C) was used as an initial assessment of its sensitivity, shown in Figure 2A. For PEG-10 and 11, the initial sensitivity was determined where they evaporated the most. The initial guess was fed into an iterative solver using eq S1 to refine the sensitivity, described in the Supporting Information. Both the initial assessment and the result from the iterative solution for assessment are shown in Figure 2A, and generally agree.

To assess the validity of the sensitivity determined in Figure 2A, a subset of the individual PEG molecules were measured with both the EESI and SMPS. The size distributions in all cases were similar with a peak in the volume-weighted distribution ~ 100 nm. The range of sensitivities reported in

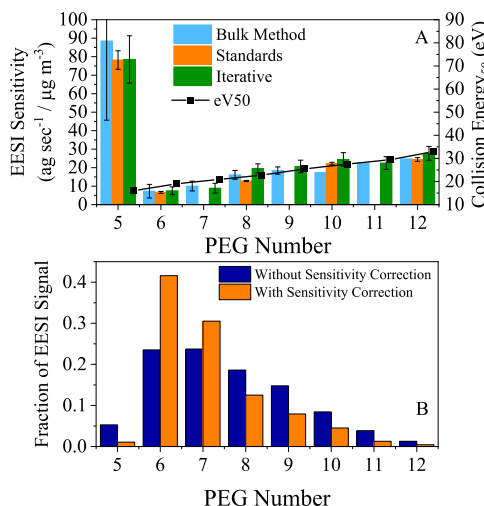


Figure 2. (A) EESI sensitivity determined from bulk standards compared to the bulk TD method and iterative-TD sensitivities (left-axis). Binding energies are shown for each PEG (right-axis). (B) Composition of PEG-300 without correction (blue) compared to the composition after correction based on EESI sensitivity (orange).

Figure 2A from the TD-EESI measurements (both bulk and iterative method) agrees well with the sensitivity measured when directly atomizing known species, providing confidence that the TD-EESI method can determine the sensitivity of unknown mixtures.

The variability in the sensitivity in Figure 2A exhibits both high sensitivity at low TD temperatures and a steadily increasing sensitivity with temperature for larger molecules. The steadily increasing trend in Figure 1C from 40 to 120 °C may relate to the increased binding energy of Na^+ to large molecules, which can more efficiently form bonds with the Na^+ stabilizing the adduct. The binding energy of Na^+ to ethers (e.g., dimethyl ether, crown ethers, etc.) increases with the number of ether groups present on the molecule.²⁴ The increased binding energy was experimentally verified using MS/MS measurements performed on PEG-300 (right-axis on Figure 2A). While the increase in the binding energy of the PEG- Na^+ adducts explains the trend in sensitivity at temperatures >40 °C, the outsized sensitivity of PEG5, which evaporates <40 °C, remains unexplained. We measured the temperature of the EESI inlet to be 42 °C in the spray region and 37 °C in the tube leading to the spray, both of which are above room temperature. Therefore, this region likely facilitates evaporation of the most volatile components such as PEG-5. Because the EESI has considerably higher sensitivity toward the gas-phase compared to the particle phase, thereby explaining the higher sensitivity of PEG-5.²⁵ To test this hypothesis, experiments were performed in which the temperature of the inlet capillary was lowered from 275 to 110 °C, thereby decreasing the temperature on the EESI inlet to room temperature. When PEG-300 was passed through the TD at 30–40 °C the sensitivity of the PEG5 decreased to ~5 ($\text{ag sec}^{-1}/(\mu\text{g m}^{-3})$).

The mass spectrum shown in Figure 1A represents the measurements of the EESI toward PEG-300 without any correction for the variation in sensitivity observed. Given the dependence of sensitivity on molecular identity in Figure 1B, it is clear that applying a single bulk sensitivity does not properly represent the composition of PEG-300. Averaged sensitivities

shown in Figure 2A (iterative solution) are applied to the EESI data, converting ag s^{-1} into $\mu\text{g m}^{-3}$ of each component present. Figure 2B shows the relative fraction of each PEG unit before and after the correction, increasing the contribution of the lowest sensitivity species (PEG-6 and 7) while decreasing the contribution to the rest of the distribution. Furthermore, after the correction, the agreement with the measured mass improves, as shown in Figure S5.

Application to Secondary Organic Aerosol. Here, we apply the method for quantification of volatility-resolved fractions of PEG-300 to a complex atmospherically relevant organic aerosol. Secondary organic aerosol (SOA) was chosen as a mixture of complex unknown species because SOA is generated by oxidation reactions that produce a wide range of chemical species, akin to an organic chemistry experiment gone awry, as clearly illustrated in Figure 3A. Additionally, SOA

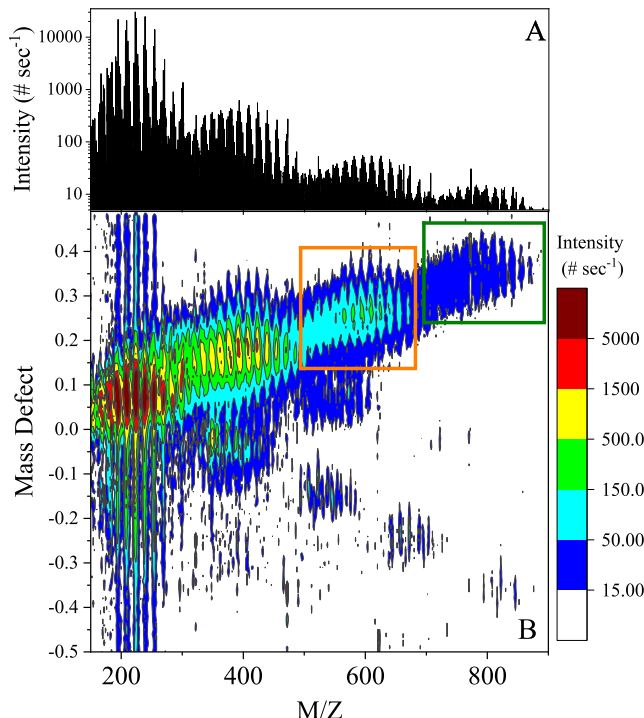


Figure 3. (A) Mass spectrum from α -pinene SOA measured by the EESI. (B) Mass defect plot of the same mass spectrum. Trimers highlighted in orange, tetramers highlighted in green.

should mostly comprise water-soluble species detectable by the EESI, rendering differences in extraction efficiency negligible.²⁶ Figure 3B shows a mass defect plot of α -pinene SOA generated via ozonolysis. The groups of ions in Figure 3B with a negative mass defect that continues to decrease with m/z correspond to $[\text{M}]_{\text{Na},\text{I}_{x-1}}^+$ clusters; these have signals that are orders of magnitude lower than the typical $[\text{M}]\text{Na}^+$ adducts and are removed from further analysis. For the remaining ($[\text{M}]\text{Na}^+$) ions, Figure 3B clearly shows regions corresponding to monomers, dimers, trimers (orange box), and tetramers (green box). Given the range of molecules present, they may be differentiated by volatility, and their relative sensitivities assessed.

The composition of SOA directly measured by the EESI is shown in Figure S4, where it is classified in terms of carbon and oxygen. Monomers comprise 60% of the signal, dimers 32.7%, trimers 6.2%, and tetramers 1.0%. Passing the SOA

through the TD results in selective evaporation of volatility-segregated classes of SOA components. Molecular formulae were aggregated according to their evaporation behavior (shown in Figure S5A,B). The classes are split into monomers (C_{7-10}) and dimers (C_{15-20}), and further aggregated according to the number of oxygen atoms present (e.g., $C_{7-10}H_xO_{3-5,6-7,8+}$ and $C_{15-20}H_yO_{4-7,10+}$). Figure 4A shows

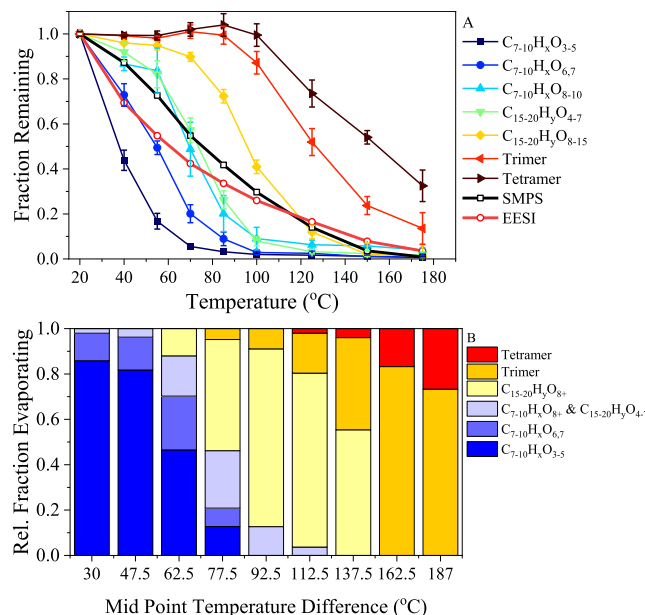


Figure 4. (A) Fraction remaining of the SMPS mass concentration (size distributions are found in Figure S7), EESI measured composition, and aggregated classes of α -pinene SOA (from triplicate measurements). (B) Relative fraction of species evaporating between TD steps for a single measurement.

each class of molecules and the temperature-dependent evaporation of the aggregated molecular species. Between 20 and 70 °C, monomers evaporate from the particle phase, with those having the fewest oxygens evaporating at the lowest temperatures. The distinction between $C_{7-10}H_xO_{3-5}$ and $C_{7-10}H_xO_{6,7}$ is not straightforward since both classes of molecules predominantly evaporate between 20 and 55 °C. However, the $C_{7-10}H_xO_{6,7}$ class evaporates at systematically higher temperatures and have a much larger fraction evaporating between 55 and 70 °C. Dimers evaporate between 70 and 125 °C, again with higher oxygen number corresponding to higher evaporation temperatures. Trimers and tetramers mostly evaporate above 125 °C. These results show that the dimers, trimers, and tetramers are effectively the only species left in the particle phase after 70–85 °C meaning that ~50% of the aerosol must be oligomers based on Figure 4A.

The comparison between the total EESI signal and the SMPS for SOA (Figure 4A), shows that the EESI signal does not perfectly follow the aerosol mass concentration in response to evaporation, with the discrepancies consistent with those observed for PEG-300. Using Figure 4A, the positive bias in the EESI again comes from the most volatile species (less oxygenated monomers) evaporating due to high inlet capillary temperatures and low volatile species (trimers and tetramers), while the negative bias is centered on highly oxygenated monomers and dimers. The relatively good separation in the evaporation temperatures between the major molecular classes

(e.g., $C_{7-10}H_xO_{3-5}$ and $C_{15-20}H_yO_{8+}$) facilitates quantification of their sensitivities by comparison with SMPS, analogous to the PEG experiments, which will more accurately determine the oligomeric fraction. Based on the chosen classes, the highly oxygenated monomers ($C_{7-10}H_xO_{8+}$) and low oxygenated dimers ($C_{15-20}H_xO_{4-7}$) were aggregated for the sensitivity determination, but are shown as separate species below.

As done for PEG, the availability of volatility-resolved sensitivities provides a means of correcting the measured carbon distribution. The bulk method was used to generate an initial guess of the sensitivity of the molecular classes of α -pinene SOA, and an iterative approach was used to refine the sensitivity (as described in the Supporting Information and used for PEG-300). For molecular classes that dominated an individual evaporation period ($C_{7-10}H_xO_{3-5}$, $C_{15-20}H_yO_{8+}$, and trimers), the bulk sensitivity during that period was taken as an initial guess in the model. Otherwise, the model was initialized using the temperature range in which molecular classes exhibited the most evaporation (40–70 °C for $C_{7-10}H_xO_{6,7}$; 55–85 °C for $C_{7-10}H_xO_{8+}/C_{15-20}H_yO_{4-7}$). Figure 5A includes

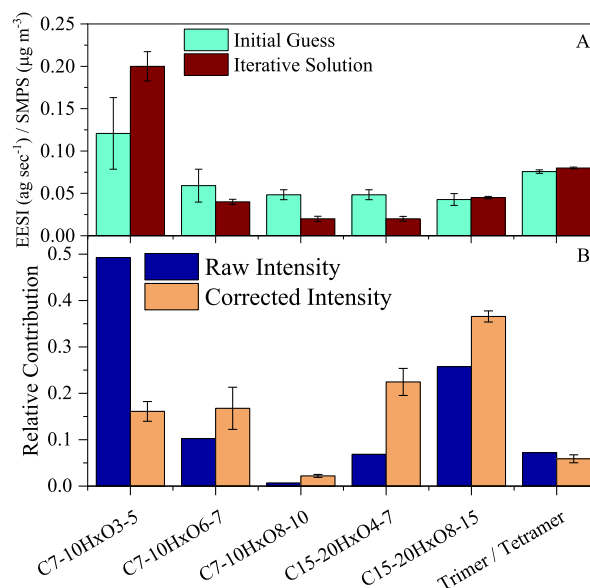


Figure 5. (A) Sensitivity for the different molecular classes of α -pinene SOA based on bulk sensitivities (initial guess) and after the iterative solution. (B) Relative contribution of each molecular class before and after the sensitivity correction using the iterative solution.

the determined sensitivity for each molecular class (including the initial guess for comparison) using this method, in the units of $(\text{ag sec}^{-1})/(\mu\text{g m}^{-3})$. Figure 5B highlights the change in the relative contributions of the different molecular classes using the iterative correction in Figure 5A. The species which did not dominate the evaporation in any specific period had relatively large errors, and results in the large error bars in Figure 5B. When shown as EESI mass concentration after sensitivity correction, there is good agreement with the measured SMPS mass concentration (Figure S8) and largely falls on the 1:1 line.

The sensitivity correction in Figure 5B increases the contribution of dimers and highly oxygenated monomers ($O_{n \geq 6}$) relative to all other components of the SOA. In terms of relative abundance, the correction based on sensitivity decreased the monomer fraction from 60.2 to 37.4%, increased

the dimers from 32.7 to 56.1%, and decreased the higher order oligomers from 7.2 to 6.4%. The estimated fractions of oligomers are consistent with the simple view in Figure 4A, where oligomers are ~50% of the aerosol. After using the iterative approach, the fractions of oligomers are greater than the rough estimate because low oxygenated dimers are beginning to evaporate between 55 and 70 °C. Changes to the less oxygenated monomers ($C_{7-10}H_xO_{3-5}$) drives the large decrease in the relative intensity of the monomer distribution (Figure 5B), while all dimer classes are enhanced with the correction. Overall, the correction fundamentally changes the picture of the composition of α -pinene SOA from one dominated by monomers to one where dimers are the most important contributor to the SOA mass. Previously, oligomers (dimers, trimers, tetramers, etc.) have been observed in atmospheric gas-phase and particle-phase measurements,^{10,13,17,27} but no method assigned bulk concentrations of oligomers in SOA until now.

DISCUSSION

The combination of the TD in conjunction with the EESI provides important information and constraints on the bulk quantification of organic aerosol components. Using the TD as a means to remove specific classes of molecules provides constraints on the sensitivity of these molecular classes without the need to generate specific standards associated to each molecule. Here, we use this method to extract information about the sensitivity of the EESI toward readily purchased molecules, and then expand the analysis to a mixture of unknown species using laboratory-generated SOA. This provides a basis for probing the variability in aerosol composition across OA from different sources and precursors. This method can be applied to systems for molecular sensitivities when there is not significant overlap in the volatility, as we show in the case of PEG-300. The alternative for complex systems (e.g., α -pinene SOA) is to separate species into volatility-based classes; this does not provide direct sensitivity on a molecule-by-molecule basis, but provides a generalized class sensitivity. The method cannot rule out the possibility that the sensitivity of individual molecules may vary considerably within a given volatility-based class. Despite this limitation, we show here this method can be used to provide important quantitative insights into SOA composition, such as the oligomeric fraction of α -pinene SOA. Overall, these results demonstrate the importance of dimers on the overall composition of α -pinene SOA and prescribe a method with which to correct for sensitivity differences among the different components of OA. Many studies have shown that oligomers are important constituents of SOA,⁸ but no study has been able to quantify this fraction.

It is also important to note that the use of SMPS-measured evaporated mass as reference means that this method is only applicable to complex mixtures consisting of species that are water soluble and readily binding to Na^+ . In the atmosphere, there are aerosol components that the EESI may not ionize (e.g., hydrocarbon-like organic aerosol), which would render this method inoperable. The good agreement between the binding energy of the PEGs and EESI sensitivity derived from both the single components and TD-EESI method could provide a way forward to determine the EESI sensitivity on a molecule-by-molecule basis. Empirical determination of binding energies through collision induced dissociation measurements could provide a means to determine EESI sensitivity,

and will be explored further in subsequent flow tube and chamber measurements. Though, this needs to be systematically determined with known species rather than complex mixtures because the binding energies likely varies based on the carbon backbone of the molecule, as shown for isomers for both α -pinene SOA and trimethyl benzene SOA.⁴

The TD-EESI combination additionally provides the possibility to model the volatility and saturation vapor concentrations of the molecules observed, however, the scope of this paper is to highlight its use to constrain the sensitivity of the EESI toward monoterpene SOAs. Future work will include extracting the volatility parameters on a molecule-by-molecule basis. Additionally, this method will be applied to the broad differences in the composition arising from different monoterpene SOAs.

ASSOCIATED CONTENT

Supporting Information

The Supporting Information is available free of charge at <https://pubs.acs.org/doi/10.1021/acs.analchem.3c00441>.

Description of iterative solution for sensitivity, experimental design, schematic of the EESI inlet, average size distributions measured by the SMPS for PEG-300, fraction evaporating from PEG-300 for each specific species, comparison of the EESI mass concentrations with sensitivity conversion (in Figure 2A) from $ag\ s^{-1}$ to $\mu g\ m^{-3}$ to the measured SMPS mass concentration, fraction remaining of the monomer and dimer regions aggregated by oxygen number as a function of TD temperature, mass weighted size distributions, and mass concentration comparison (PDF)

AUTHOR INFORMATION

Corresponding Author

David M. Bell – Laboratory of Atmospheric Chemistry, Paul Scherrer Institute, Villigen 5232, Switzerland;  orcid.org/0000-0002-3958-2138; Email: david.bell@psi.ch

Authors

Jun Zhang – Laboratory of Atmospheric Chemistry, Paul Scherrer Institute, Villigen 5232, Switzerland

Jens Top – Laboratory of Atmospheric Chemistry, Paul Scherrer Institute, Villigen 5232, Switzerland;  orcid.org/0000-0003-3318-4451

Sophie Bogler – Laboratory of Atmospheric Chemistry, Paul Scherrer Institute, Villigen 5232, Switzerland

Mihnea Surdu – Laboratory of Atmospheric Chemistry, Paul Scherrer Institute, Villigen 5232, Switzerland;  orcid.org/0000-0003-1815-2750

Jay G. Slowik – Laboratory of Atmospheric Chemistry, Paul Scherrer Institute, Villigen 5232, Switzerland

Andre S. H. Prevot – Laboratory of Atmospheric Chemistry, Paul Scherrer Institute, Villigen 5232, Switzerland;  orcid.org/0000-0002-9243-8194

Imad El Haddad – Laboratory of Atmospheric Chemistry, Paul Scherrer Institute, Villigen 5232, Switzerland;  orcid.org/0000-0002-2461-7238

Complete contact information is available at:

<https://pubs.acs.org/doi/10.1021/acs.analchem.3c00441>

Author Contributions

D.M.B. wrote the manuscript with contributions from all authors. D.M.B., J.Z., M.S., and J.T. performed chamber experiments. J.Z. and S.B. performed PEG measurements. D.M.B. and J.Z. analyzed the EESI data. J.T. performed collision-induced dissociation measurements. All authors gave approval to the final version of the manuscript.

Notes

The authors declare no competing financial interest.

ACKNOWLEDGMENTS

This work was supported by the Swiss National Science Foundation (grant 09802.01.03, 200021_213071, 206021_198140, and 200020_188624) as well as the European Union's Horizon 2020 research and innovation programme through the ATMO-ACCESS Integrating Activity under grant agreement no. 101008004 and the Marie Curie doctoral network under grant no. HORIZON-MSCA-2021-DN-01.

REFERENCES

- (1) (a) Koop, T.; Bookhold, J.; Shiraiwa, M.; Pöschl, U. *Phys. Chem. Chem. Phys.* **2011**, *13*, 19238–19255. (b) Shiraiwa, M.; Ammann, M.; Koop, T.; Pöschl, U. *Proc. Natl. Acad. Sci. U.S.A.* **2011**, *108*, 11003–11008.
- (2) (a) Dolovich, M. B.; Dhand, R. *Lancet* **2011**, *377*, 1032–1045. (b) Douafer, H.; Andrieu, V.; Brunel, J. M. *J. Controlled Release* **2020**, *325*, 276–292.
- (3) Daellenbach, K. R.; Uzu, G.; Jiang, J.; Cassagnes, L.-E.; Leni, Z.; Vlachou, A.; Stefenelli, G.; Canonaco, F.; Weber, S.; Segers, A.; et al. *Nature* **2020**, *587*, 414–419.
- (4) Wang, D. S.; Lee, C. P.; Krechmer, J. E.; Majluf, F.; Tong, Y.; Canagaratna, M. R.; Schmale, J.; Prévôt, A. S. H.; Baltensperger, U.; Dommen, J.; et al. *Atmos. Meas. Tech.* **2021**, *14*, 6955–6972.
- (5) Jimenez, J. L.; Canagaratna, M. R.; Donahue, N. M.; Prevot, A. S. H.; Zhang, Q.; Kroll, J. H.; DeCarlo, P. F.; Allan, J. D.; Coe, H.; Ng, N. L.; et al. *Science* **2009**, *326*, 1525–1529.
- (6) (a) Mohr, C.; Thornton, J. A.; Heitto, A.; Lopez-Hilfiker, F. D.; Lutz, A.; Riipinen, I.; Hong, J.; Donahue, N. M.; Hallquist, M.; Petäjä, T.; et al. *Nat. Commun.* **2019**, *10*, 4442. (b) Stolzenburg, D.; Fischer, L.; Vogel, A. L.; Heinritzi, M.; Schervish, M.; Simon, M.; Wagner, A. C.; Dada, L.; Ahonen, L. R.; Amorim, A.; et al. *Proc. Natl. Acad. Sci. U.S.A.* **2018**, *115*, 9122–9127.
- (7) (a) Simon, M.; Dada, L.; Heinritzi, M.; Scholz, W.; Stolzenburg, D.; Fischer, L.; Wagner, A. C.; Kürten, A.; Rörup, B.; He, X. C.; et al. *Atmos. Chem. Phys.* **2020**, *20*, 9183–9207. (b) Heinritzi, M.; Dada, L.; Simon, M.; Stolzenburg, D.; Wagner, A. C.; Fischer, L.; Ahonen, L. R.; Amanatidis, S.; Baalbaki, R.; Baccarini, A.; et al. *Atmos. Chem. Phys.* **2020**, *20*, 11809–11821. (c) Ye, Q.; Wang, M.; Hofbauer, V.; Stolzenburg, D.; Chen, D.; Schervish, M.; Vogel, A.; Mauldin, R. L.; Baalbaki, R.; Brilke, S.; et al. *Environ. Sci. Technol.* **2019**, *53*, 12357–12365. (d) Frege, C.; Ortega, I. K.; Rissanen, M. P.; Praplan, A. P.; Steiner, G.; Heinritzi, M.; Ahonen, L.; Amorim, A.; Bernhammer, A.-K.; Bianchi, F.; et al. *Atmos. Chem. Phys.* **2018**, *18*, 65–79. (e) Lehtipalo, K.; Yan, C.; Dada, L.; Bianchi, F.; Xiao, M.; Wagner, R.; Stolzenburg, D.; Ahonen, L. R.; Amorim, A.; Baccarini, A.; et al. *Sci. Adv.* **2018**, *4*, No. eaau5363.
- (8) (a) Dommen, J.; Metzger, A.; Duplissy, J.; Kalberer, M.; Alfara, M. R.; Gascho, A.; Weingartner, E.; Prevot, A. S. H.; Verheggen, B.; Baltensperger, U. *Geophys. Res. Lett.* **2006**, *33*, L13805. (b) Kalberer, M.; Paulsen, D.; Sax, M.; Steinbacher, M.; Dommen, J.; Prevot, A. S. H.; Fisseha, R.; Weingartner, E.; Frankevich, V.; Zenobi, R.; et al. *Science* **2004**, *303*, 1659–1662. (c) Laskin, A.; Laskin, J.; Nizkorodov, S. A. *Environ. Chem.* **2012**, *9*, 163–189. (d) Walser, M. L.; Desyaterik, Y.; Laskin, J.; Laskin, A.; Nizkorodov, S. A. *Phys. Chem. Chem. Phys.* **2008**, *10*, 1009–1022. (e) Bateman, A. P.; Walser, M. L.; Desyaterik, Y.; Laskin, J.; Laskin, A.; Nizkorodov, S. A. *Environ. Sci. Technol.* **2008**, *42*, 7341–7346.
- (9) (a) Müller, M.; Piel, F.; Gutmann, R.; Sulzer, P.; Hartungen, E.; Wisthaler, A. *Int. J. Mass Spectrom.* **2020**, *447*, 116254. (b) Leglise, J.; Müller, M.; Piel, F.; Otto, T.; Wisthaler, A. *Anal. Chem.* **2019**, *91*, 12619–12624. (c) Eichler, P.; Müller, M.; D'Anna, B.; Wisthaler, A. *Atmos. Meas. Tech.* **2015**, *8*, 1353–1360. (d) Huang, W.; Saathoff, H.; Shen, X.; Ramisetty, R.; Leisner, T.; Mohr, C. *Environ. Sci. Technol.* **2019**, *53*, 1165–1174. (e) Mohr, C.; Lopez-Hilfiker, F. D.; Yli-Juuti, T.; Heitto, A.; Lutz, A.; Hallquist, M.; D'Ambro, E. L.; Rissanen, M. P.; Hao, L.; Schobesberger, S.; et al. *Geophys. Res. Lett.* **2017**, *44*, 2958–2966.
- (10) Wu, C.; Bell, D. M.; Graham, E. L.; Haslett, S.; Riipinen, I.; Baltensperger, U.; Bertrand, A.; Giannoukos, S.; Schoonbaert, J.; El Haddad, I.; et al. *Atmos. Chem. Phys.* **2021**, *21*, 14907–14925.
- (11) Lopez-Hilfiker, F. D.; Pospisilova, V.; Huang, W.; Kalberer, M.; Mohr, C.; Stefenelli, G.; Thornton, J. A.; Baltensperger, U.; Prevot, A. S. H.; Slowik, J. G. *Atmos. Meas. Tech.* **2019**, *12*, 4867–4886.
- (12) Lee, C. P.; Surdu, M.; Bell, D. M.; Lamkaddam, H.; Wang, M.; Ataei, F.; Hofbauer, V.; Lopez, B.; Donahue, N. M.; Dommen, J.; et al. *Atmos. Meas. Tech.* **2021**, *14*, 5913–5923.
- (13) Pospisilova, V.; Bell, D. M.; Lamkaddam, H.; Bertrand, A.; Wang, L.; Bhattu, D.; Zhou, X.; Dommen, J.; Prevot, A. S. H.; Baltensperger, U.; et al. *Environ. Sci. Technol.* **2021**, *55*, 6936–6943.
- (14) Surdu, M.; Pospisilova, V.; Xiao, M.; Wang, M.; Mentler, B.; Simon, M.; Stolzenburg, D.; Hoyle, C. R.; Bell, D. M.; Lee, C. P.; et al. *Environ. Sci.: Atmos.* **2021**, *1*, 434–448.
- (15) Patriarca, C.; Balderrama, A.; Može, M.; Sjöberg, P. J. R.; Bergquist, J.; Tranvik, L. J.; Hawkes, J. A. *Anal. Chem.* **2020**, *92*, 14210–14218.
- (16) The pre-publication history for this paper can be accessed here: <http://www.biomedcentral.com/1471-2466/14/31/prepub>. (a) Qi, L.; Chen, M.; Stefenelli, G.; Pospisilova, V.; Tong, Y.; Bertrand, A.; Hueglin, C.; Ge, X.; Baltensperger, U.; Prévôt, A. S. H.; et al. *Atmos. Chem. Phys.* **2019**, *19*, 8037–8062. (b) Stefenelli, G.; Pospisilova, V.; Lopez-Hilfiker, F. D.; Daellenbach, K. R.; Hüglin, C.; Tong, Y.; Baltensperger, U.; Prévôt, A. S. H.; Slowik, J. G. *Atmos. Chem. Phys.* **2019**, *19*, 14825–14848.
- (17) Bell, D. M.; Wu, C.; Bertrand, A.; Graham, E.; Schoonbaert, J.; Giannoukos, S.; Baltensperger, U.; Prevot, A. S. H.; Riipinen, I.; El Haddad, I.; et al. *Atmos. Chem. Phys.* **2022**, *22*, 13167–13182.
- (18) Liu, X.; Day, D. A.; Krechmer, J. E.; Brown, W.; Peng, Z.; Zieman, P. J.; Jimenez, J. L. *Commun. Chem.* **2019**, *2*, 98.
- (19) Rovelli, G.; Jacobs, M. I.; Willis, M. D.; Rapf, R. J.; Prophet, A. M.; Wilson, K. R. *Chem. Sci.* **2020**, *11*, 13026–13043.
- (20) (a) Krieger, U. K.; Siegrist, F.; Marcolla, C.; Emanuelsson, E. U.; Göbel, F. M.; Bilde, M.; Marsh, A.; Reid, J. P.; Huisman, A. J.; Riipinen, I.; et al. *Atmos. Meas. Tech.* **2018**, *11*, 49–63. (b) Ylisirniö, A.; Barreira, L. M. F.; Pullinen, I.; Buchholz, A.; Jayne, J.; Krechmer, J. E.; Worsnop, D. R.; Virtanen, A.; Schobesberger, S. *Atmos. Meas. Tech.* **2021**, *14*, 355–367.
- (21) (a) Bell, D. M.; Imre, D.; T Martin, S.; Zelenyuk, A. *Phys. Chem. Chem. Phys.* **2017**, *19*, 6497–6507. (b) Wilson, J.; Imre, D.; Beránek, J.; Shrivastava, M.; Zelenyuk, A. *Environ. Sci. Technol.* **2015**, *49*, 243–249.
- (22) Vaden, T. D.; Imre, D.; Beránek, J.; Shrivastava, M.; Zelenyuk, A. *Proc. Natl. Acad. Sci. U.S.A.* **2011**, *108*, 2190–2195.
- (23) Platt, S. M.; El Haddad, I.; Zardini, A. A.; Clairotte, M.; Astorga, C.; Wolf, R.; Slowik, J. G.; Temime-Roussel, B.; Marchand, N.; Ježek, I.; et al. *Atmos. Chem. Phys.* **2013**, *13*, 9141–9158.
- (24) (a) Armentrout, P. B. *Int. J. Mass Spectrom.* **1999**, *193*, 227–240. (b) More, M. B.; Ray, D.; Armentrout, P. B. *J. Phys. Chem. A* **1997**, *101*, 831–839.
- (25) Lee, C. P.; Surdu, M.; Bell, D. M.; Dommen, J.; Xiao, M.; Zhou, X.; Baccarini, A.; Giannoukos, S.; Wehrle, G.; Schneider, P. A.; et al. *Atmos. Meas. Tech.* **2022**, *15*, 3747–3760.
- (26) Clark, C. H.; Nakao, S.; Asa-Awuku, A.; Sato, K.; Cocker, D. R. *Aerosol Sci. Technol.* **2013**, *47*, 1374–1382.

- (27) (a) Romonosky, D. E.; Li, Y.; Shiraiwa, M.; Laskin, A.; Laskin, J.; Nizkorodov, S. A. *J. Phys. Chem. A* **2017**, *121*, 1298–1309.
(b) Pospisilova, V.; Lopez-Hilfiker, F. D.; Bell, D. M.; El Haddad, I.; Mohr, C.; Huang, W.; Heikkinen, L.; Xiao, M.; Dommen, J.; Prevot, A. S. H.; et al. *Sci. Adv.* **2020**, *6*, No. eaax8922.

□ Recommended by ACS

Development of a High-Field “Brick” Mass Spectrometer with Extended Mass Range and Capable of Characterizing Native Proteins

Hongjia Zhang, Wei Xu, et al.

AUGUST 31, 2023

ANALYTICAL CHEMISTRY

READ ▶

Investigation of Zero-/High-Field Ion Mobility Orthogonal Separation Using a Hyphenated DMA–FAIMS System and Validation of the Two-Temperature Theory at Arbitrary F...

Viraj D. Gandhi, Carlos Larriba-Andaluz, et al.

MAY 12, 2023

ANALYTICAL CHEMISTRY

READ ▶

Improving the Sensitivity of Fourier Transform Mass Spectrometer (Orbitrap) for Online Measurements of Atmospheric Vapors

Runlong Cai, Mikael Ehn, et al.

NOVEMBER 07, 2022

ANALYTICAL CHEMISTRY

READ ▶

Effect of Humidity on the Mobilities of Small Ions in Ion Mobility Spectrometry

Izabela Wolańska, Jarosław Puton, et al.

MAY 23, 2023

ANALYTICAL CHEMISTRY

READ ▶

Get More Suggestions >